Earthquakes and Structures, *Vol. 16, No. 6 (2019) 757-769*
DOI: https://doi.org/10.12989/eas.2019.16.6.757

Shear strength prediction of PRC coupling beams with low span-to-depth ratio

Jianbo Tian*[1,2], Dandan Shen[1], Shen Li[1,2], Zheng Jian[1,2], Yunhe Liu[1,2] and Wengeng Ren[1]

[1]School of Civil Engineering and Architecture, Xi'an University of Technology, No. 5,Jinhua Road, Xi'an, Shaanxi, China
[2]State Key Laboratory Base of Eco-hydraulic Engineering in Arid Area, Xi'an University of Technology, No. 5,Jinhua Road, Xi'an, Shaanxi, China

(Received February 2, 2019, Revised April 8, 2019, Accepted April 10, 2019)

Abstract. The seismic performance of a coupled shear wall system is governed by the shear resistances of its coupling beams. The plate-reinforced composite (PRC) coupling beam is a newly developed form of coupling beam that exhibits high deformation and energy dissipation capacities. In this study, the shear capacity of plate-reinforced composite coupling beams was investigated. The shear strengths of PRC coupling beams with low span-to-depth ratios were calculated using a softened strut-and-tie model. In addition, a shear mechanical model and calculating method were established in combination with a multi-strip model. Furthermore, a simplified formula was proposed to calculate the shear strengths of PRC coupling beams with low span-to-depth ratios. An analytical model was proposed based on the force mechanism of the composite coupling beam and was proven to exhibit adequate accuracy when compared with the available test results. The comparative results indicated that the new shear model exhibited more reasonable assessment accuracy and higher reliability. This method included a definite mechanical model and reasonably reflected the failure mechanisms of PRC coupling beams with low span-to-depth ratios not exceeding 2.5.

Keywords: shear strength; plate-reinforced composite coupling beam; low span-to-depth ratio; softened strut-and-tie model; softened effects

1. Introduction

A coupling beam is an important seismic energy dissipation member of coupled shear wall systems, and its ductility and energy dissipation abilities significantly influence the seismic performance of the shear wall structure. An embedded steel plate significantly improves the shear strength of a plate-reinforced composite (PRC) coupling beam. The relative test data of PRC coupling beams are insufficient to date, and thus there is a paucity of a good model and calculation method to calculate the shear capacity of PRC coupling beams. The aforementioned issue necessitates further investigation.

The shear failure of reinforced concrete beams undergoes concrete cracking, and the most commonly used methods that are currently used to calculate the ultimate shear strength of concrete beams include the truss model (Ramirez and Breen 1991), strut-and-tie model (Foster and Malik 2002), plastic theoretical model (Hoang and Nielsen 1998), and modified compression field theory (Collins 1986). The calculation of shear capacity is relatively complicated owing to the different stress mechanisms of different forms of composite coupling beams. Subedi (1989) According to the equilibrium condition, the shear bearing is analyzed. Based on the test and numerical analysis, Lam (2006) proposed a design method for PRC coupling beams. Superiority of the steel coupling beams is demonstrated through detailed evaluations of local and global responses computed for a number of recorded and artificially generated ground motions by Habib and Roja (2016). Three proposed steel plate-reinforced high toughness-concrete (PRHTC) coupling beams with different span-to-depth ratios (l/h=1.0, 1.5, and 2.0) and various steel plate reinforcement ratios were tested by Hou (2018) all three PRHTC coupling beams behaved in a ductile manner with good hysteretic behavior and large energy-dissipating capacity. This significantly affects the calculation of the bending and shear bearing capacity of steel-concrete composite coupling beams. A combination of the British concrete code (BS 8110 1997) was used to calculate the shear capacity of a composite beam. Subedi and Baglin (1997), Cheng (2004) performed cyclic and monotonic loading tests on PRC continuous beams. In the testing of PRC coupling beams, the bulk of specimens suffered flexural shear failure. The ultimate shear bearing capacity of the composite beam (V_u) is superimposed on the shear bearing capacity of the reinforced concrete (V_{RC}) calculated by BS 8110 (1997). The shear bearing capacity of reinforced concrete V_{RC} is divided into two parts, namely the shear capacity of stirrups V_v and V_c, by considering the action of the longitudinal reinforcement. Similarly, the shear capacity of composite beam is calculated by combining the American concrete association code (ACI 318 2014) and American steel structure association specification (AISC 1999). The ultimate shear bearing

∗Corresponding author, Lecturer
E-mail: tianjianbo@xaut.edu.cn

http://www.techno-press.com/journals/eas&subpage=7
ISSN: 2092-7614 (Print), 2092-7622 (Online)

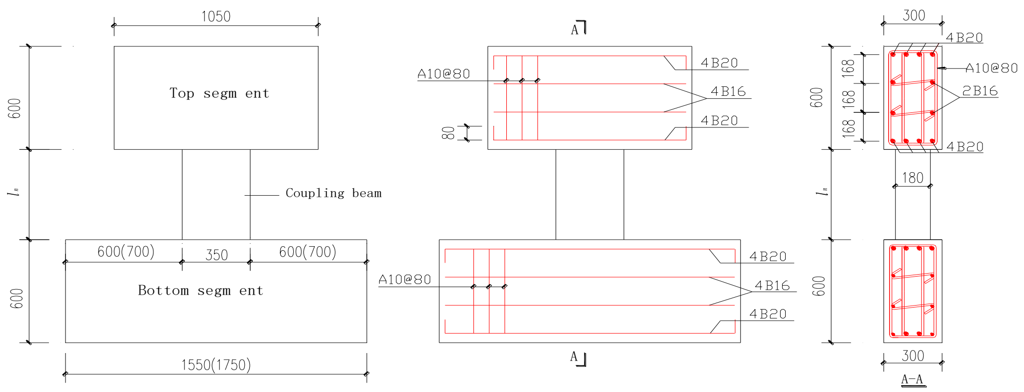

Notes: Span-to-depth ratio of specimen PRC-CB4 is 0.9, and bottom segment length increases to 1750 mm

(a) Specimen geometries and reinforcement details of the constraint segment

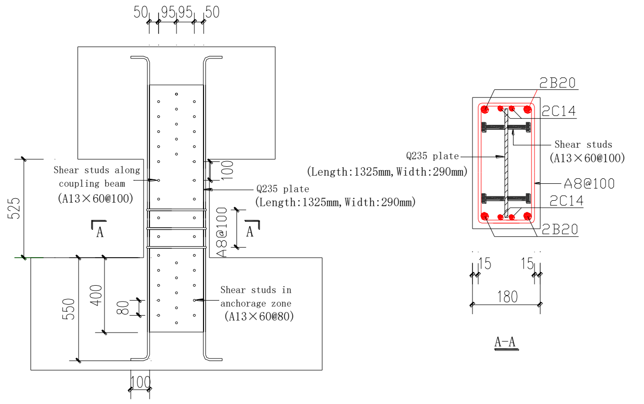

(b) Reinforcement details of the PRC-CB1 to PRC-CB3 coupling beam

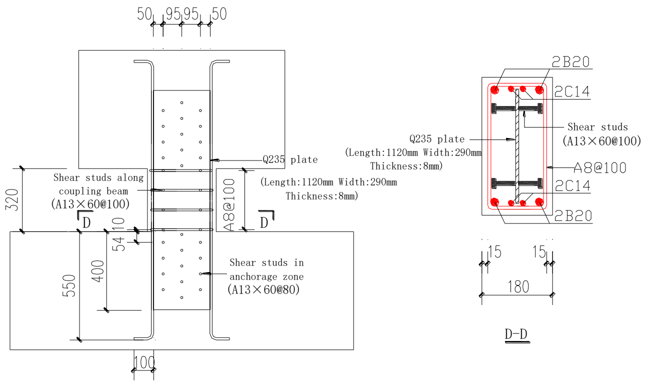

(c) Reinforcement details of the PRC-CB4 coupling beam

Notes: Span-to-depth ratio of specimen PRC-CB1 to PRC-CB3 are 1.5, and the steel plate thickness is 6mm, 8mm and 10mm respectively.

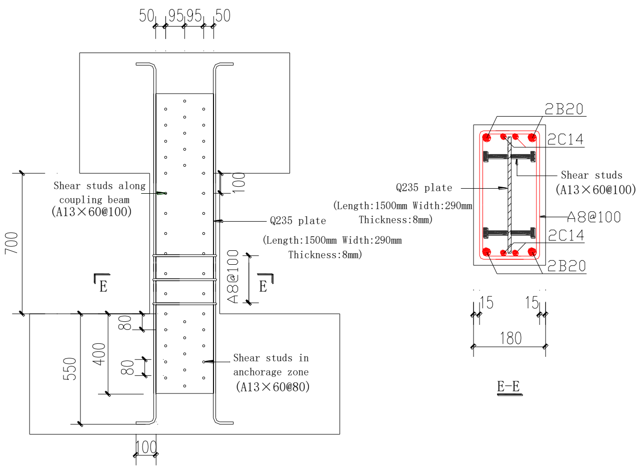

(d) Reinforcement details of the PRC-CB5 coupling beam

Fig. 1 Dimensions (mm) and reinforcement details of the specimens

capacity of the composite beam (V_n) comp is superimposed on the shear bearing capacity of the steel plate (V_n)s as calculated by AISC (1999) and shear bearing capacity of the reinforced concrete (V_n) RC as calculated by ACI 318.

With respect to the contribution of steel plate to shear bearing capacity, there are differences while considering various calculation methods. When the coupling beam corresponds to a coupling beam with a low span-to-depth ratio *ln/h* not exceeding 2.5, the coupling beam belongs to the deep beam category, and the deep beam belongs to the '*D* region'. The softened truss model, plastic theory, and simplified modified field theory require the deformation of the component to satisfy the deformation coordination conditions, and thus it is difficult to apply the same to calculate the shear bearing capacity of the *D* region (Wong and Kuang 2014). The application of beam-column nodes (Park and Mosalam 2012), deep beams, brackets and low shear wall (Hwang *et al.* 2001a, b) indicated that the softened strut-and-tie model accurately predicts the bearing capacity of these types of *D* regions.

In this study, the shear capacity of plate-reinforced composite coupling beams is investigated. The shear strengths of PRC coupling beams with low span-to-depth ratios were calculated using a softened strut-and-tie model. In addition, a shear mechanical model and calculating method are established in combination with a multi-strip model. Furthermore, a simplified formula to calculate the shear strength of a PRC coupling beam with a low span-to-depth ratio is proposed. The suggested analytical model is verified using test data from 37 PRC coupling beams with low span-to-depth ratios. The theoretical results are compared with those obtained with the softened strut-and-tie model and the code. Good agreement is achieved between the test results and prediction results.

2. Experimental programme

2.1 Test specimens

Reversed cyclic loading tests were performed on five PRC coupling beam specimens (PRC-CB1 to PRC-CB5) with low span-to-depth ratios. The width of the upper and lower constraints was 300 mm, and the amount of reinforcement at the end of the constraints was relatively significant. There were sufficient constraints and stiffness to simulate the shear wall to prevent excessive deformation at the end, and this affects the accuracy of the coupling beam tests. The width and height of the test coupling beams were 180 mm and 350 mm, respectively, and different span-to-depth ratios were realised by adjusting the span of the coupling beams.

In order to examine the shear bearing capacity of PRC coupling beams, the longitudinal reinforcement ratios in coupling beams increased based on the assumption that the flexural load-carrying capacity exceeded the designed shear bearing capacity. Two types of steel bars were used in the upper and lower longitudinal reinforcement of the coupling beams in the specimens as follows: grades HRB335 (nominal yield strength f_y=335 MPa), and HRB400 (nominal yield strength f_y=400 MPa) The longitudinal reinforcement ratios of the coupling beams corresponded to 1.65%. Stirrup meshes with a diameter of 8 mm (D8) were placed in the coupling beams at 100-mm intervals. The strength grade of the stirrups was HPB300 (nominal yield strength f_y=300 MPa). The stirrup ratios of the coupling beams were 0.56%.

The anchor length of each specimen was 1.14 times the beam height (400 mm), and shear studs were welded on the beam spans and anchorage zones. We increased the number of anchorage zones of the shear studs to enhance the bonding with concrete. The effect of anchorage length of steel plates on the shear bearing capacities of PRC coupling beams with low span-to-depth ratios were not considered in this study. The dimensions and reinforcement details of the specimens are shown in Fig. 1, and the primary parameters are listed in Table 1.

The strength grade of the concrete in all specimens was C40 (nominal cubic compressive strength f_{cu}=40 MPa, and design value of axial compressive strength f_c=19.1 MPa). The cubic strength of the concrete ($f_{cu,t}$) measured at the time of specimen testing was 58.16 MPa, and this corresponds to the average strength of eight cubes with a size of 150 mm. The material properties of the rebars and steel plates are listed in Table 2.

Table 1 Specimen parameters

Spec. No.	l_n/h	d_w (mm)	t_w (mm)	ρ_p (%)
PRC-CB1	1.5	290	6	3.07
PRC-CB2	1.5	290	8	4.09
PRC-CB3	1.5	290	10	5.11
PRC-CB4	0.9	290	8	4.09
PRC-CB5	2.0	290	8	4.09

Notes: l_n/h denotes the span-to-depth ratio of the coupling beam, L_n denotes the clear span of the coupling beam, and h denotes the section height of the coupling beam, d_w denotes the height of the steel plate, t_w denotes the thickness of the steel plate, and ρ_p denotes the sectional steel plate ratio of the coupling beam.

Table 2 Material properties of the rebars and steel plates

Material type	Steel type	Thickness (Diameter) (mm)	Yield strength f_y (MPa)	Ultimate strength f_u (MPa)
Steel plate	Q235	6	245	395
		8	280	425
		10	235	393
Longitudinal reinforcement of the coupling beam	HRB335	20	470	655
Longitudinal reinforcement of the coupling beam	HRB400	14	450	633
Stirrup of the coupling beam	HPB300	8	320	473
Middle rebars of the constraint segment	HRB335	16	448	628
Stirrup of the constraint segment	HPB300	10	591	695

2.2 Test setup and loading protocol

The test setup is shown in Fig. 2. In order to simulate the antisymmetric forces acting on the contra-flexure point at mid-span of the coupling beam, reversed cyclic loading was applied using a 1000 kN servo-controlled hydraulic actuator through the rigid arm with the line of action of the applied shear force passing through the beam. Thus, the coupling beam was loaded with a constant shear force along the span and a bending moment that linearly varied with the point of inflection located at the mid-span, and this simulated the conditions in an actual building (Tsonos 2007).

Fig. 3 shows the test loading protocol. Force-controlled cycling loading was applied until the specimens yielded,

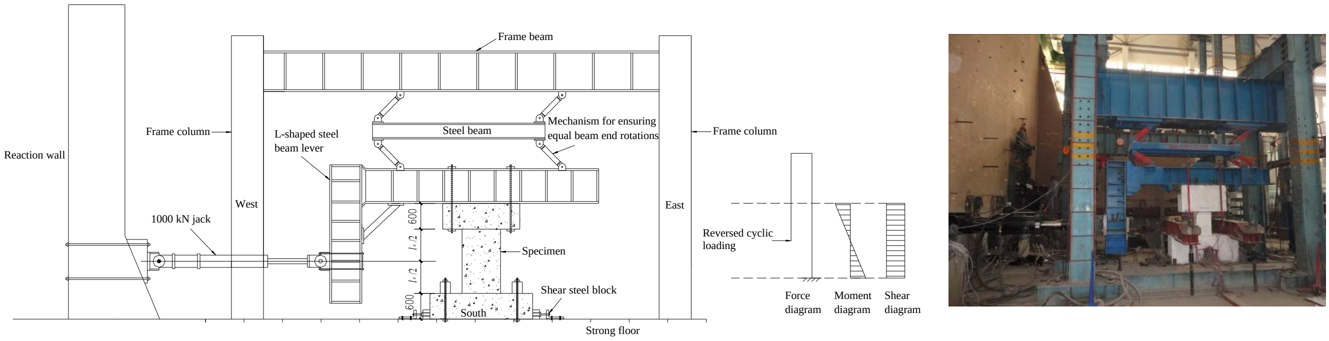

(a) Test setup and force diagram of the coupling beam (b) Test setup

Fig. 2 Test setup

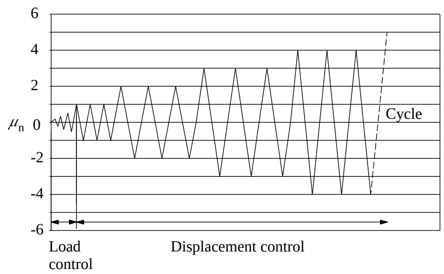

Fig. 3 Loading protocol

and the applied forces were cycled once at each level in 40 kN increments. The specimen was expected to yield When the load-displacement curve of the specimen reached an evident turning point. The displacements in the subsequent cycles were controlled when the specimen was displaced to a nominal ductility factor μ_n=1 for one cycle and subsequently at each successive nominal ductility factor for three cycles as shown in Fig. 3. In order to prove the shear effect of embedded steel plates in PRC coupling beams, the test was terminated when the peak load obtained in the first cycle with nominal ductility level fell below $0.85V_{max}$ or when the beam rotation (θ) of the coupling beams reached approximately 1/11. The test specimen was subsequently considered to exhibit failure.

3. Experimental results and discussion

3.1 Hysteretic response

Fig. 4 shows the hysteretic curves of shear force (V) relative to the relative line displacement (Δ) at both ends of the coupling beams for each specimen. After the specimens yield, the bearing capacities of the coupling beams continues to increase with increases in the beam end displacement, and the hysteretic loops become increasingly plump. Because of the rapid development of diagonal cracks in the concrete, all the specimens continued to load stably after reaching the peak load. This indicates that the

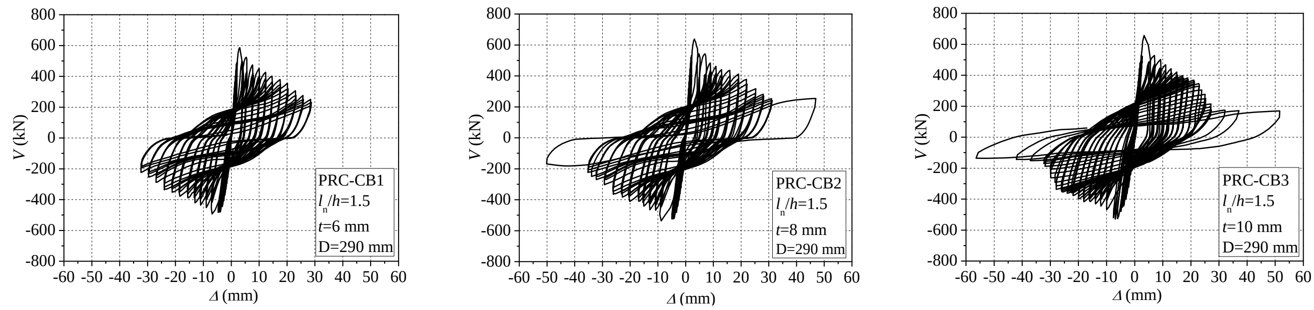

(a) PRC-CB1 (b) PRC-CB2 (c) PRC-CB3

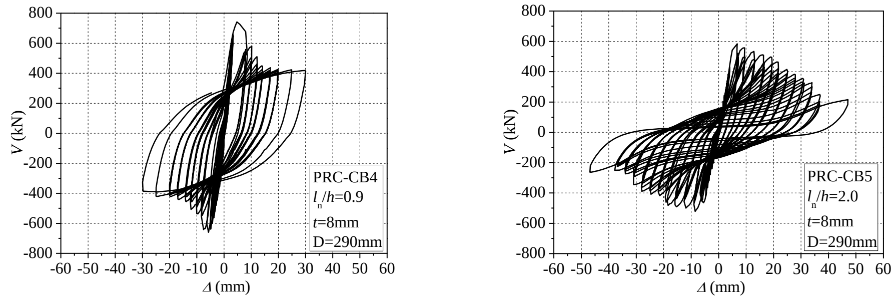

(f) PRC-CB4 (g) PRC-CB5

Fig. 4 Hysteretic responses of specimens

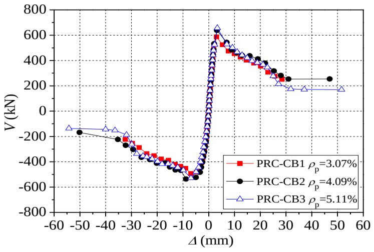

(a) Sectional steel plate ratio

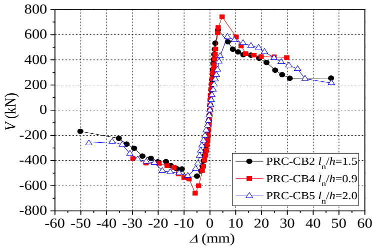

(b) Span-to-depth ratio

Fig. 5 Influence of the parameters on envelope curves

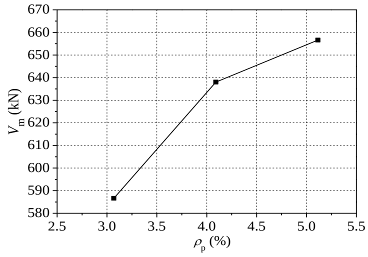

(a) Sectional steel plate ratio

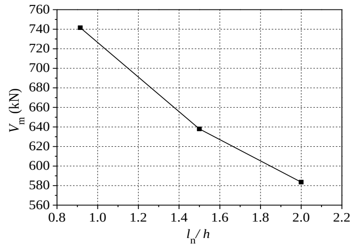

(b) Span-to-depth ratio

Fig. 6 Influence of the parameters on shear capacity

steel plate exhibits good performance in terms of both holding and energy dissipation capacities. After the formation of diagonal cracks, stress redistribution occurs inside the specimen with increases in the crack width. The concrete does not bear any stress due to cracking, and the internal forces that the concrete is subjected to are borne by the steel plate, which corresponds to the primary shear material. With increases in the steel plate thickness and span-to-depth ratio, the hysteretic loops become plumper, and the energy dissipation capacity increases.

3.2 Strength and ductility

Fig. 5 shows the envelope curves of shear force (V) versus relative line displacement (Δ) at both ends of the coupling beams for each specimen. The envelope curve gradient of each specimen in the elastic stage is steep. The rising trend is essentially identical, and this indicates that the embedded steel plate increases the initial stiffness of PRC coupling beams. When the steel plate heights are identical, the bearing capacity of PRC coupling beams gradually increases with increases in the steel plate thickness. In the descending section, the influence of steel plate thickness on the changing trends of envelope curves is not evident. The envelope curve gradient of PRC-CB5 is lower in the elastic stage. With increases in the span-to-depth ratios, the descending section of the PRC coupling beam envelope curves is shallower. The bearing capacity of the PRC coupling beams increases with decreases in the span-to-depth ratios. Decreases in the span-to-depth ratio increase the rate of increase in the specimen carrying capacity.

Table 3 presents the experimental results for all five specimens. The bearing capacity, displacement, chord rotation angle, and measured shear-compression ratios of the specimens are obtained at different loading stages. The

Table 3 Experimental results at the main stages

Specimen	Loading direction	Yield point			Peak point			Failure point			μ	$\bar{\mu}$
		V_y (kN)	Δ_y (mm)	θ_y (rad)	V_m (kN)	Δ_m (mm)	θ_m (rad)	V_u (kN)	Δ_u (mm)	θ_u (rad)		
PRC-CB1	Positive	526.98	2.40	1/219	586.60	3.05	1/172	498.61	6.57	1/80	2.74	3.61
	Negative	435.17	3.06	1/172	493.30	6.89	1/76	419.31	13.12	1/40	4.29	
PRC-CB2	Positive	571.45	2.51	1/209	638.00	3.22	1/163	542.30	7.03	1/75	2.80	3.36
	Negative	485.28	3.66	1/143	536.53	8.81	1/60	456.05	13.72	1/38	3.75	
PRC-CB3	Positive	570.55	2.68	1/196	656.60	3.38	1/156	558.11	6.16	1/85	2.30	2.58
	Negative	454.35	4.19	1/125	528.95	6.90	1/76	449.60	11.56	1/45	2.76	
PRC-CB4	Positive	668.80	3.46	1/93	741.50	4.76	1/67	630.28	8.54	1/37	2.47	2.26
	Negative	552.13	3.75	1/85	659.98	5.70	1/56	560.99	7.76	1/41	2.07	
PRC-CB5	Positive	516.49	5.55	1/126	583.49	6.77	1/103	495.97	18.96	1/37	3.41	3.44
	Negative	471.47	5.83	1/120	521.67	8.54	1/82	443.42	20.24	1/35	3.47	

Notes: V_y denotes the yield shear load, V_m denotes the peak shear load, V_u denotes the failure shear load, Δ_y denotes the relative line displacement at the yield shear load, Δ_m denotes the relative line displacement at the peak shear load, Δ_u denotes the relative line displacement at the failure shear load, θ_y denotes the actual yield chord rotation angle, θ_m denotes the chord rotation angle at peak shear load, and θ_u denotes the ultimate measured chord rotation angle, μ denotes the maximum ductility factor, and $\bar{\mu}$ denotes the average value of maximum ductility factor.

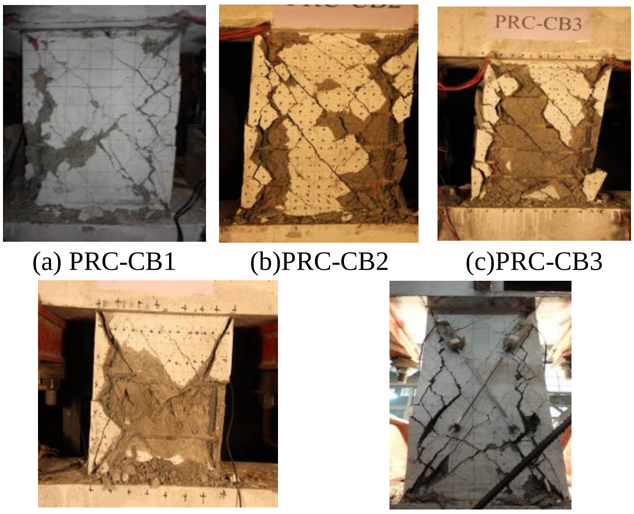

(a) PRC-CB1 (b)PRC-CB2 (c)PRC-CB3

(d) PRC-CB4 (e) PRC-CB5

Fig. 7 The final damage form of the test specimens

maximum ductility factors are defined as the ultimate rotations divided by the actual yield rotations obtained from the test ($\mu=\theta_u/\theta_y$). The average value of the maximum ductility factor ($\bar{\mu}$) is expressed as follows

$$\bar{\mu}=\left(\left|\Delta_u^+\right|+\left|\Delta_u^-\right|\right)/\left(\left|\Delta_y^+\right|+\left|\Delta_y^-\right|\right) \tag{1}$$

Fig. 6 shows the influence of different parameters on the shear capacity of a PRC coupling beam with a low span-to-depth ratio. With increases in the sectional steel plate ratio, the average value of the maximum ductility factor ($\bar{\mu}$) of PRC coupling beams gradually decreases. This indicates that increases in the sectional area of the steel plate increase the bending resistance moment and decrease the ductility at the limit state. The displacement ductility factors of PRC coupling beams increase with increases in the span-to-depth ratios. The displacement ductility factors of PRC-CB2 and PRC-CB5 are 1.49 and 1.52 times that of PRC-CB4, respectively.

3.3 Experimental damage characteristics

In this experiment, diagonal shear failure occurred in PRC-CB1 to PRC-CB3 and PRC-CB4 in five PRC low span to depth ratio coupling beams, and shear bond failure occurred in specimen PRC-CB5. The main reason for this failure mode is to study the contribution of the steel plate to the shear capacity of the coupling beam, and increase the reinforcement of the longitudinal reinforcement in the coupling beam, so that the bending capacity of the coupling beam is greater than the shear capacity. The final failure mode of thecoupling beam is shown in Fig. 7.

4. Softened strut-and-tie model

4.1 Shear resisting mechanism

The shear mechanism of reinforced concrete frame joints is composed of the following three parts: diagonal

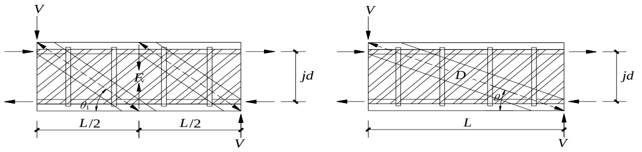

(a) Vertical mechanism (b) Diagonal strut mechanism

Fig. 8 Shear resisting mechanisms of a PRC coupling beam with low span-to-depth ratio

(strut action), horizontal, and vertical (truss action) mechanism when using the softened strut-and-tie model to carry out the shear analysis. The horizontal mechanism consists of a horizontal tie rod and two gentle strut rods. The shear strength of a PRC coupling beam with a low span-to-depth ratio is calculated using the softened strut-and-tie model. The horizontal tie rod is composed of the longitudinal constructional reinforcement of the coupling beams. The results of our tests and results obtained from PRC coupling beams indicate that the longitudinal constructional reinforcement does not significantly influence shear strength. When the span-to-depth ratio is $0.75\leq\lambda\leq1.60$ (λ is the span-to-depth ratio of coupling beam), the coupling beam is mainly composed of a diagonal strut mechanism and a vertical mechanism to resist shear force. With increases in the span-to-depth ratio λ, the effect of the diagonal strut mechanism reduces and the effect of the vertical mechanism increases. Therefore, in this study, when the shear analysis of the PRC coupling beams with low span-to-depth ratios is performed, the shearing mechanism includes the diagonal strut mechanism and vertical mechanism as shown in Fig. 8.

For the rectangular section of a PRC coupling beam with a low span-to-depth ratio, the level arm jd of the rectangular section is estimated as follows

$$jd=d-\frac{kd}{3} \tag{2}$$

where d denotes the effective depth of the coupling beam section, k denotes the coefficient representing the ratio of depth of concrete compression. The coefficient k is estimated as follows (Hsu and Mo 2010)

$$k=\sqrt{\begin{array}{l}\left[n\rho_{\mathrm{s}}+(n-1)\rho_{\mathrm{s}}'+\left|(m-1)\rho_{\mathrm{p}}\right|\right]^2\\ +2\left[n\rho_{\mathrm{s}}+(n-1)\rho_{\mathrm{s}}'\dfrac{d'}{d}+\left|(m-1)\rho_{\mathrm{p}}\right|\left(\dfrac{d_1'}{d}+\dfrac{d_{\mathrm{w}}}{2d}\right)\right]\end{array}}-\left[n\rho_{\mathrm{s}}+(n-1)\rho_{\mathrm{s}}'+\left|(m-1)\rho_{\mathrm{p}}\right|\right] \tag{3}$$

where ρ_{s} denotes the ratio of the tension reinforcement, $\rho_{\mathrm{s'}}$ denotes the ratio of the compression reinforcement, ρ_{p} denotes the ratio of steel plate; n and m denote the modular ratio of elasticity, $n=E_{\mathrm{ss}}/E_{\mathrm{c}}$, $m=E_{\mathrm{sp}}/E_{\mathrm{c}}$, E_{ss} denotes the elasticity modulus of reinforcement, E_{sp} denotes the elasticity modulus of steel plate, E_{c} denotes the elasticity modulus of concrete; d' denotes the distance between the extreme compression fibre to the centroid of the compression reinforcement, $d_{1'}$ denotes the distance

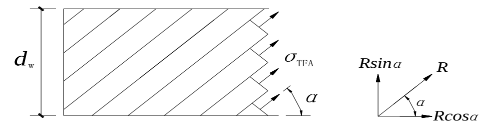

Fig. 9 Multi-strip model for the encased steel plate of the PRC coupling beam

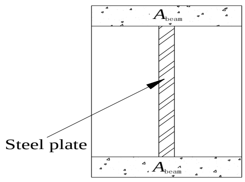

Fig. 10 Cross-section of the PRC coupling beam

between the extreme compression fibre to the edge of the steel plate, and d_w denotes the depth of the steel plate.

According to Fig. 8, the inclination angle of the strut in diagonal mechanism θ and inclination angle of the strut in vertical mechanism θ_1, are defined as follows, respectively (Lian *et al.*2017a, b)

$$\theta = \tan^{-1}\left(\frac{jd}{L}\right) \tag{4}$$

$$\theta_1 = \tan^{-1}\left(\frac{2jd}{L}\right) \tag{5}$$

where L denotes the span length of the coupling beam.

The direction of the principal compressive stress of the concrete is assumed as coincident with the direction of the diagonal concrete strut. The effective area of the diagonal strut A_{strut} is as follows

$$A_{strut}=a_s b \tag{6}$$

where b denotes the width of the beam, and a_s denotes the depth of the diagonal strut that depends on the end conditions, and is estimated as follows

$$a_s = \sqrt{(kd)^2 + (kd)^2} \tag{7}$$

4.2 Multi-strip model in the encased steel plate

As shown in the experimental observations, the encased steel plate buckles in shear with a sinusoidal wave form in the PRC coupling beam. This indicates that the steel plate resists the shear in the form of a diagonal tension field. Therefore, a multi-strip model proposed by Thorburn *et al.* (1983a, b) is adopted to idealise diagonal tension stresses in the steel plate by a series of inclined strips with angles of inclination as shown in Fig. 9.

The angle of inclination of the strip α is defined as follows

$$\alpha = \tan^{-1}\left[\frac{1+\dfrac{t_w d_w}{2A_{wall}}}{1+\dfrac{t_w L}{A_{beam}}}\right]^{\frac{1}{4}} \tag{8}$$

where A_{beam} denotes the cross-sectional area of the concrete above or below the encased steel plate as shown in Fig. 10. Furthermore, A_{wall} denotes the cross-sectional area of the adjacent shear wall, t_w denotes the thickness of the steel plate, d_w denotes the depth of the steel plate, and L denotes the span length of the coupling beam (Wang *et al.*2017a, b).

The resultant force for all the strips F_p is as follows

$$F_p = \sigma_{TFA} t_w d_w / \cos\alpha \tag{9}$$

where σ_{TFA} denotes the diagonal tension stresses of a strip.

Additionally, the vertical and horizontal components of F_p are respectively expressed as follows

$$F_{pv} = F_p \sin\alpha \tag{10}$$

$$F_{ph} = F_p \cos\alpha \tag{11}$$

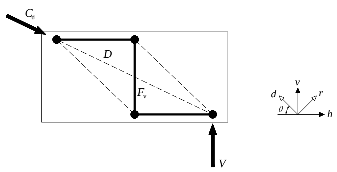

Fig. 11 Forces in struts and ties

4.3 Equilibrium conditions

The total force in the vertical direction of the coupling beam is resisted by the diagonal strut mechanism and vertical mechanism as shown in Fig. 11. The total force in the vertical direction V_{bv} is defined as follows

$$V_{bv} = -D\sin\theta + F_v \tag{12}$$

where D denotes the compression force in the diagonal concrete strut, F_v denotes the total force in the vertical tie.

The presence of the encased steel plate also contributes to the vertical tie, and the force of the vertical tie subsequently corresponds to the combination of the steel plate and stirrup (Wang and Shi 2015), and F_v is expressed as follows

$$\begin{aligned} F_v &= F_{stirrup} + F_p \sin\alpha \\ &= E_{stirrup} A_{stirrup} \varepsilon_v + E_p (t_w d_w / \cos\alpha) \varepsilon_v \sin\alpha \end{aligned} \tag{13}$$

where $F_{stirrup}$ denotes the total force in the stirrup.

According to (Hwang *et al.* 2001a, b), the shear forces resisted by the two mechanisms are determined as follows

$$D = \frac{-1}{\sin\theta}\left(\frac{R_d}{R_d + R_v}\right)V_{bv} \tag{14}$$

$$F_v = \left(\frac{R_v}{R_d + R_v}\right)V_{bv} \tag{15}$$

$$R_d = 1 - \gamma_v \tag{16}$$

$$R_v = \gamma_v = \frac{2\cot\theta - 1}{3} \quad \text{for} \quad 0 \le \gamma_v \le 1 \tag{17}$$

where R_d and R_v are respectively the ratio of the shear force to the diagonal strut mechanism and vertical mechanism, γ_v denotes the vertical shear of vertical tie without horizontal tie.

At the nodal zone, the diagonal compression strength C_{ds} by the concrete strut A_{strut} (which is governed by the concrete softening) is estimated as follows

$$C_{ds} = \sigma_{ds} A_{strut} \tag{18}$$

$$\sigma_{ds} = \frac{1}{A_{strut}}\left[D - \frac{\cos(\theta_1 - \theta)}{\sin\theta_1} F_v\right] \tag{19}$$

Owing to the presence of the encased steel plate in the PRC coupling beam, the steel plate contributes to the diagonal compressive strength C_{du} of the strut, and the diagonal strength is not affected by the concrete softening properties. Thus, the expression is follows (Tian *et al.* 2019a, b)

$$C_{du} = f_c' A_{du} \tag{20}$$

$$A_{du} = a_s (m-1) t_w \frac{\cos\alpha}{\sin\alpha} \tag{21}$$

where a_s denotes the depth of the diagonal strut, $a_s = \sqrt{(kd)^2 + (kd)^2}$; f_c' denotes the compressive strength of the concrete cylinder, and m denotes the modular ratio of elasticity where $m = E_{sp}/E_c$.

Therefore, the predicted shear strength of a PRC coupling beam with a low span-to-depth ratio is as follows

$$V_{Predicted} = (C_{ds} + C_{du})\sin\theta \tag{22}$$

4.4 Constitutive laws of materials

As shown in the experimental observations in a previous study and those in the present study, the failure model of the steel-plate encased concrete coupling beams in the presence of stirrups corresponds to diagonal failure with concrete crushing in the compression zone. Hence, the softening of concrete should not be neglected, and it is believed that the shear strength of the section is governed by the softened concrete.

According to Zhang and Hsu (1998), the softened stress-strain relationship of the cracked concrete is expressed as follows

$$\sigma_d = -\zeta f_c'\left[2\left(\frac{-\varepsilon_d}{\zeta\varepsilon_0}\right) - \left(\frac{-\varepsilon_d}{\zeta\varepsilon_0}\right)^2\right] \quad \text{for} \quad \frac{-\varepsilon_d}{\zeta\varepsilon_0} \le 1 \tag{23a}$$

$$\sigma_d = -\zeta f_c'\left[1 - \left(\frac{-\varepsilon_d/(\zeta\varepsilon_0) - 1}{2/\zeta - 1}\right)^2\right] \quad \text{for} \quad \frac{-\varepsilon_d}{\zeta\varepsilon_0} > 1 \tag{23b}$$

$$\zeta = \frac{5.8}{\sqrt{f_c'}} \cdot \frac{1}{\sqrt{1 + 400\varepsilon_r}} \le \frac{0.9}{\sqrt{1 + 400\varepsilon_r}} \tag{24}$$

where σ_d denotes the principal stress of concrete at the d direction, ζ denotes the softening coefficient of concrete, ε_d and ε_r denote the main compressive strain and main tensile strain of concrete, respectively. Furthermore, ε_0 denotes the concrete cylindrical strain that corresponds to the cylinder strength, and it is defined approximately as follows

$$\varepsilon_0 = 0.002 + 0.001\left(\frac{f_c' - 20}{80}\right) \quad \text{for} \quad 20 \le f_c' \le 100 \tag{25}$$

The stress-strain relationship of the stirrups and steel plate are assumed as elastic-perfectly plastic and is expressed as follows

$$f_s = E_s \varepsilon_s \quad \text{for} \quad \varepsilon_s < \varepsilon_y \tag{26a}$$

$$f_s = f_y \quad \text{for} \quad \varepsilon_s \ge \varepsilon_y \tag{26b}$$

where E_s denotes the elasticity of stirrup E_{st} or steel plate E_{sp}, f_y denotes the yield stress of the stirrup f_{yt} or steel plate f_{yp}, and ε_y denotes the yield strain of the stirrup ε_{yt} or steel plate ε_{yp}.

4.5 Compatibility condition

The two-dimensional thin-film element should satisfy the Mohr circle strain coordination condition. The basic coordination equation corresponds to the first order strain invariant equation. To satisfy the compatibility, the sum of the normal strains in two perpendicular directions (Fig. 11) is an invariant such that the following equation is applicable (Liang and Xing 2018)

$$\varepsilon_r + \varepsilon_d = \varepsilon_h + \varepsilon_v \tag{27}$$

where ε_h denotes the average normal strain in the h-direction, and ε_v denotes the average normal strain in the v-direction.

4.6 Solution procedure

The procedure for using the softened strut-and-tie model to calculate the shear strength of the PRC coupling beam with low span-to-depth ratio is as follows.

Step 1: The procedure commences with the selection of V_{bv}, and D and F_v are subsequently estimated by Eqs. (14)-(17), and ε_v and σ_{ds} are estimated by Eqs. (13)-(19), respectively. Additionally, ε_h is set as zero due to the inactivity of the horizontal mechanisms.

Step 2: By selecting ε_d, ε_r is calculated from Eq. (27). Subsequently, the softening coefficient ζ is calculated from Eq. (24). The maximum compressive strength σ_d of the cracked concrete is determined from Eqs. (23a)-(23b).

Step 3: By comparing $|\sigma_{ds}|$ calculated in Step 1 and $|\sigma_d|$ calculated in Step 2, if $|\sigma_{ds}|<|\sigma_d|$, then we increase the value of V_{bv} and repeat Steps 1 and 2 until $|\sigma_{ds}|\ge|\sigma_d|$.

Step 4: If $|\varepsilon_d|<|\zeta_{\varepsilon 0}|$, we increase the value of ε_d and repeat Steps 2 and 3 until $|\varepsilon_d|\ge|\zeta_{\varepsilon 0}|$. Subsequently, the diagonal compression strength C_{ds} by the concrete strut is calculated from Eq. (18).

Step 5: Using Eqs. (20)-(21), the diagonal compressive strength C_{du} of the strut that is not affected by the concrete softening properties is obtained. Finally, the shear strength of the PRC coupling beam with low span-to-depth ratio is determined from Eq. (22).

Fig. 12 shows the procedures wherein the proposed model is used to calculate the shear strength of the PRC coupling beam.

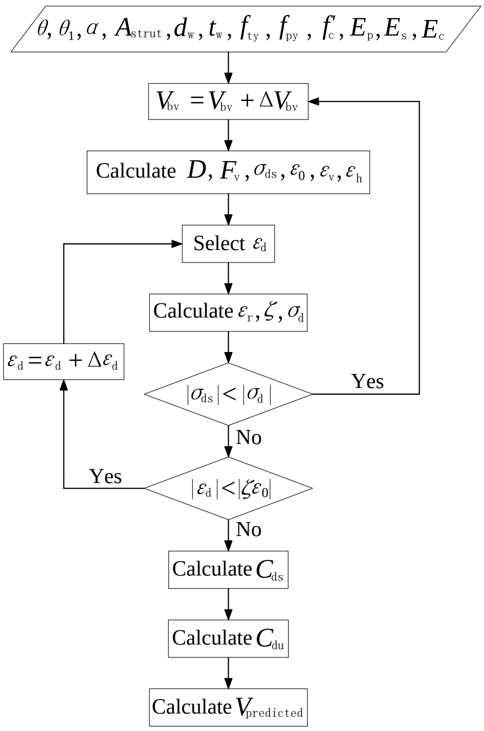

Fig. 12 Flow chart of the proposed modelling procedure

5. A simplified method of the softened strut-and-tie model

As shown in the experimental observations of the stirrup strain and steel plate internal force of the reference (Lam 2006) and our research group, the stirrups do not fully yield when the specimens reach the ultimate load, and the ratio of stirrups to shear is lower than that of the steel plate. Therefore, the shear effect of stirrups is neglected while calculating the shear bearing capacity of the coupling beam. However, when the diagonal cracks occur in PRC coupling beam specimens, the stirrups restrict shear inclined cracks, and thereby limit the crack width while continuing to play a certain role in providing constraints for oblique compression concrete. Therefore, the minimum number of stirrups should be allocated according to the structure while designing the PRC coupling beam.

According to the proposed modelling procedure of the softened strut-and-tie model, the shear capacity V_u of PRC coupling beam with a low span-to-depth ratio should be composed of the diagonal compression strength by the concrete strut and diagonal compressive strength of the strut by the steel plates. Additionally, given the softening effect of concrete, the shear bearing capacity V_u of a PRC coupling beam with a low span-to-depth ratio is expressed as follows

$$\begin{aligned} V_u &= (k_c \zeta f_c' A_{strut} + C_{du}) \sin\theta \\ &= \left[k_c \zeta f_c' a_s b + f_c' a_s (m-1) t_w \frac{\cos\alpha}{\sin\alpha} \right] \sin\theta \end{aligned} \tag{28}$$

where ζ denotes the softening coefficient of concrete compressive strength calculated from reference (Xing *et al.* 2011a, b) and is defined as follows

$$\zeta \approx 3.35/\sqrt{f_c'} \le 0.52 \tag{29}$$

The coefficient k_c in Eq. (28) reflects the contribution of stirrups and diagonal concrete strut to the shear capacity V_u of the PRC coupling beam. Based on the experimental data analysis, k_c is estimated as follows

$$k_c = 1.2 \tag{30}$$

By substituting Eqs. (29)-(30) into Eq. (28), a simplified formula of the softened strut-and-tie model is expressed as follows (Seongwoo *et al.*2014a, b)

$$V_u = \left[4.02\sqrt{f_c'} \cdot b + f_c'(m-1) t_w \frac{\cos\alpha}{\sin\alpha} \right] a_s \sin\theta \tag{31}$$

where a_s denotes the depth of the diagonal strut, $a_s = \sqrt{(kd)^2 + (kd)^2}$; f_c' denotes the compressive strength of concrete cylinder, m denotes the modular ratio of elasticity, $m=E_{sp}/E_c$; b denotes the width of the beam, t_w denotes the thickness of the steel plate; θ is calculated from Eq. (4), and α is calculated from Eq. (8).

6. Verification

To verify the accuracy of the proposed model in this study, the experimental data of 37 PRC coupling beams under unidirectional loading or reversed cyclic loading are collected, and the selection principle is that diagonal shear, shear bond, or shear compression failures occur in PRC coupling beams. Table 4 presents the basic information for each specimen, experimental results, and shear strength of PRC coupling beams calculated by the softened strut-and-tie model (SSTM), simplified method of the softened strut-and-tie model (S-SSTM), China technical specification of steel-reinforced concrete structure by YB9082, British Code (BS 8110 1997), and American Code (ACI 318 2014, AISC 1999). The actual strength of concrete is calculated. To indicate the accuracy and conservative bias of each approach, the mean, standard deviation (STDEV), and coefficient of variation (COV) for the strength ratios are shown in Table 4.

The standard deviation and coefficient of variation calculated from the softened strut-and-tie model (SSTM) are the lowest. Good agreement between the test results and prediction results from the SSTM is achieved. The method includes a definite mechanical model that reasonably reflects the failure mechanisms of PRC coupling beams with span-to-depth ratios not exceeding 2.5.

The means for the strength ratios of the test value to the theoretical value calculated by the American Code (ACI 318 2014, AISC 1999) and British Code (BS 8110 1997) are 1.16 and 1.23, respectively, and the standard deviation is 0.32. The calculated results are reliable and in good agreement with the experimental values. However, they are more discrete than the V_{test}/V_{cal} calculated by the softened strut-and-tie model.

The mean for the strength ratios of the test value to the theoretical value calculated from the simplified method of the softened strut-and-tie model (S-SSTM) is similar to the mean calculated from the YB9082-2006. The results

Table 4 Comparison of the shear bearing capacity between test results and prediction results of the PRC coupling beams

Researcher	Specimen	l_n/h	ρ_p (%)	λ_p	ρ_s (%)	f_{cu} (MPa)	Failure modes	V_{test} (kN)	SSTM		S-SSTM		YB9082-2006		BS 8110		ACI 318 and AISC 1999	
									V_{cal} (kN)	V_{test}/V_{cal}	V_{cal} (kN)	V_{test}/V_{cal}	V_{cal} (kN)	V_{test}/V_{cal}	V_{cal} (kN)	V_{test}/V_{cal}	V_{cal} (kN)	V_{test}/V_{cal}
Cheng (2004)	1P8S-25	1.7	4.97	0.27	2.54	49	Diagonal Shear	320	355.4	0.90	372.9	0.86	315.7	1.01	259.5	1.23	271.5	1.18
	1P10S-25	1.7	6.21	0.33	2.54	49.4	Diagonal Shear	353	397.5	0.89	418.8	0.84	371.6	0.95	311.5	1.13	329.3	1.07
	1P16S-25	1.7	9.94	0.74	2.54	42.4	Diagonal Shear	520	526.3	0.99	533.2	0.98	560.1	0.93	547.3	0.95	591.2	0.88
	1P20S-25	1.7	12.43	0.91	2.54	43	Diagonal Shear	650	630.0	1.03	634.6	1.02	568.0	1.14	672.0	0.97	729.7	0.89
	1P8S-20	1.7	4.92	0.27	3.22	59.9	Diagonal Shear	427	399.1	1.07	418.9	1.02	385.6	1.11	320.1	1.33	333.9	1.28
	1P10S-20	1.7	6.15	0.34	3.22	59.9	Diagonal Shear	447	447.3	1.00	467.3	0.96	454.9	0.98	384.9	1.16	405.9	1.10
	1P20S-20	1.7	12.31	0.66	3.22	61	Shear bond	634	724.8	0.87	740.9	0.86	802.4	0.79	709.3	0.89	766.3	0.83
	2P8S-25	2.2	4.97	0.28	2.54	51	Shear bond	267	262.9	1.02	305.7	0.87	340.4	0.78	280.9	0.95	295.4	0.90
	2P10S-25	2.2	6.21	0.32	2.54	56.3	Shear bond	310	308.6	1.00	356.3	0.87	407.9	0.76	339.7	0.91	360.9	0.86
	2P20S-25	2.2	12.43	0.79	2.54	55.7	Shear bond	524	506.7	1.03	574.8	0.91	735.8	0.71	754.2	0.69	821.4	0.64
	2P8S-20	2.2	4.92	0.27	3.22	53.5	Shear bond	244	275.5	0.89	323.4	0.75	344.5	0.71	286.7	0.85	296.8	0.82
	2P10S-20	2.2	6.15	0.35	3.22	51.2	Shear bond	315	313.0	1.01	357.0	0.88	402.5	0.78	342.9	0.92	359.2	0.88
	2P20S-20	2.2	12.31	0.83	3.22	52.7	Shear bond	581	513.4	1.13	577.0	1.01	702.9	0.83	758.2	0.77	820.6	0.71
	3P8S-25	1.3	4.97	0.39	2.54	45.5	Diagonal Shear	430	491.7	0.87	432.4	0.99	388.7	1.11	330.8	1.30	350.7	1.23
	3P10S-25	1.3	6.21	0.48	2.54	45.9	Diagonal Shear	486	537.1	0.90	484.9	1.00	464.0	1.05	400.9	1.21	428.6	1.13
	3P20S-25	1.3	12.43	0.78	2.54	45.9	Shear bond	711	799.7	0.89	762.2	0.93	606.3	1.17	621.2	1.14	673.4	1.06
Subedi (1989)	1SP2	2.4	1.06	0.08	1.78	50	Shear bond	96	87.0	1.10	107.1	0.90	96.0	1.00	64.8	1.48	66.1	1.45
	2SP2	2.4	0.84	0.05	1.78	51.5	Shear bond	108	95.0	1.14	107.1	1.01	83.8	1.29	52.7	2.05	52.6	2.05
	3SP4	2.4	1.68	0.12	1.78	46.5	Shear bond	144	124.5	1.16	124.3	1.16	97.1	1.48	80.4	1.79	83.2	1.73
	4SP6	2.4	2.54	0.15	2.80	55	Shear compression	174	154.0	1.13	167.2	1.04	139.9	1.24	108.2	1.61	109.4	1.59
	5FP4	2.4	3.42	0.27	1.78	49.8	Shear compression	174	201.5	1.09	195.5	1.13	128.3	1.71	150.2	1.46	160.9	1.37
	6FP6	2.4	4.91	0.50	2.85	41.8	Shear compression	174	190.0	1.17	184.2	1.21	250.8	0.89	218.8	1.01	232.2	0.96
Zhang (2005)	CB25-1	2.5	1.63	0.17	1.99	42.3	Shear bond	198	188.0	1.05	181.8	1.09	308.4	0.64	239.5	0.83	246.7	0.80
Lam (2006)	SPrc-Bg	1.2	2.39	0.19	0.23	51.2	Shear compression	174	502.9	0.94	498.8	0.95	703.2	0.67	503.1	0.94	570.1	0.83
Suen (2012)	M15/P4-S1	1.5	2.46	0.25	1.61	37.8	Diagonal Shear	373.8	367.8	1.02	273.5	1.37	338.6	1.10	268.3	1.39	282.2	1.32
	M15/P6-S0	1.5	3.69	0.46	1.61	37	Shear bond	371.4	405.2	0.92	313.6	1.18	372.1	1.00	315.6	1.18	341.1	1.09
	C10/P4-S1	1.0	2.46	0.15	1.61	51.2	Diagonal Shear	431.1	456.2	0.94	403.6	1.07	319.1	1.35	239.1	1.80	251.4	1.71
	C15/P4-S1	1.5	2.46	0.15	1.61	50.5	Diagonal Shear	398.2	410.1	0.97	301.4	1.32	318.2	1.25	238.9	1.67	251.2	1.59
	C20/P4-S1	2.0	2.46	0.15	1.61	52.9	Shear bond	299.8	259.0	1.16	241.9	1.24	321.3	0.93	239.6	1.25	252.1	1.19
	C15/P4-S0	1.5	2.46	0.17	1.61	47.2	Shear bond	289.7	311.4	0.93	293.7	0.99	226.2	1.28	169.6	1.71	179.6	1.61
	C15/P4-S2	1.5	2.46	0.17	1.61	45.6	Diagonal Shear	377.8	389.3	0.97	290.0	1.30	370.3	1.02	282.9	1.34	295.9	1.28
	C15/P6-S1	1.5	3.69	0.37	1.61	46.7	Diagonal Shear	404.8	419.8	0.96	341.8	1.18	482.3	0.84	393.4	1.03	423.1	0.96

calculated from the S-SSTM are lower than those calculated from the British Code (BS 8110 1997). Nevertheless, the standard deviation is relatively low, and thus the dispersion is relatively low.

The shear strength of the specimens calculated by each design provision is plotted relative to the experimental results in Fig. 13. The points in the left upper region of the diagram indicate that the test values exceed the calculated value, and the results are reliable. The points in the lower right region of the diagram indicate that the test values are less than the calculated values, and the calculated results are unreliable. Fig. 14 shows the influence of the characteristic value λ_p of the distribution plate on the shear strength ratio V_{test}/V_{cal} of PRC coupling beam calculated by the aforementioned five methods. As shown in the figure, most of the points calculated by the American Code (ACI 318 and AISC 1999) and British Code (BS 8110) are above the straight line V_{test}/V_{cal}=1, and the results are safe. The points calculated by YB9082-2006 exhibit higher and lower fluctuations under the straight line V_{test}/V_{cal}=1. The points

Table 4 Continued

Researcher	Specimen	l_n/h	ρ_p (%)	λ_p	ρ_s (%)	f_{cu} (MPa)	Failure modes	V_{test} (kN)	SSTM		S-SSTM		YB9082-2006		BS 8110		ACI 318 and AISC 1999	
									V_{cal} (kN)	V_{test}/V_{cal}	V_{cal} (kN)	V_{test}/V_{cal}	V_{cal} (kN)	V_{test}/V_{cal}	V_{cal} (kN)	V_{test}/V_{cal}	V_{cal}(kN)	V_{test}/V_{cal}
Our group	PRC-CB1	1.5	3.07	0.17	1.65	58.2	Diagonal Shear	586.6	540.6	1.09	507.4	1.16	528.1	1.11	398.8	1.47	423.3	1.39
	PRC-CB2	1.5	4.09	0.26	1.65	58.2	Diagonal Shear	638	628.3	1.02	570.7	1.12	657.0	0.97	518.2	1.23	557.3	1.14
	PRC-CB3	1.5	5.11	0.27	1.65	58.2	Diagonal Shear	656.6	688.5	0.95	636.2	1.03	675.4	0.97	534.3	1.23	576.5	1.14
	PRC-CB4	0.9	4.09	0.26	1.65	58.2	Diagonal Shear	741.5	792.1	0.94	790.5	0.94	657.0	1.13	518.2	1.43	557.3	1.33
	PRC-CB5	2.0	4.09	0.26	1.65	58.2	Shear bond	583.5	529.5	1.10	454.5	1.28	657.0	0.89	518.2	1.13	557.3	1.05
Mean									—	1.01	—	1.04	—	1.02	—	1.23	—	1.16
STDEV									—	0.09	—	0.15	—	0.23	—	0.32	—	0.32
COV									—	0.09	—	0.15	—	0.23	—	0.26	—	0.28

Notes: l_n/h denotes the span-to-depth ratio of the coupling beam, ρ_p denotes the sectional steel plate ratio of the coupling beam, ρ_s denotes the longitudinal reinforcement ratio of the coupling beam, λ_p denotes the steel plate characteristic value of the coupling beam, $\lambda_p=(A_pf_p)/(bh_0f_c)$, f_{cu} denotes the compressive strength of the concrete cube measured in the test.

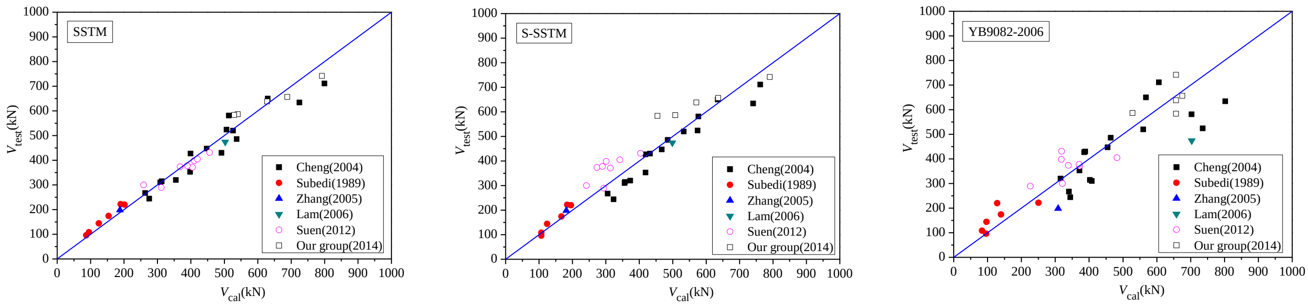

(a) SSTM (Method 1) (b) S-SSTM (Method 2) (c) YB9082-2006 (Method 3)

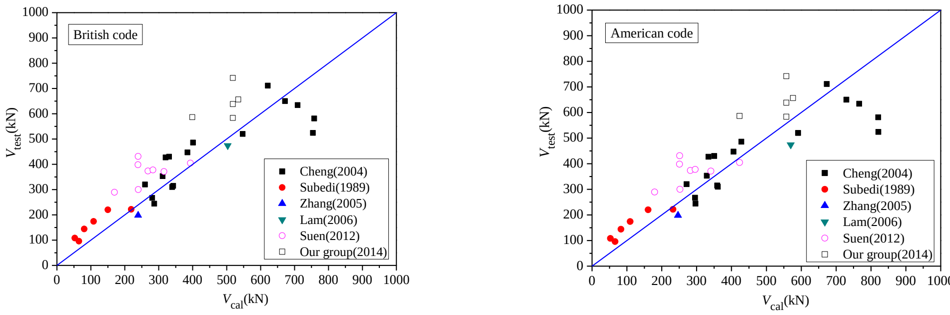

(d) British Code (BS 5950 and BS8110) (Method 4) (e) American Code (ACI 318 and AISC 1999) (Method 5)

Fig. 13 Comparison of the shear bearing capacity between test results and prediction results

calculated by SSTM and S-SSTM method along the straight line $V_{test}/V_{cal}=1$ are more uniformly distributed and exhibit less fluctuations, and this indicates that the method in this study better reflects the actual situation.

7. Conclusions

This paper presented a new mechanical model to calculate the shear strengths of PRC coupling beams with low span-to-depth ratios. The aim of the model involved combining accuracy and simplicity to evaluate resistance relative to diagonal shear, shear bond, or shear compression failures. The following conclusions were obtained based on comparisons with tests and other models:

• Based on the test results of 37 PRC coupling beams and calculation results of relevant codes, the mean for the strength ratios of the test value to the theoretical value calculated by the softened strut-and-tie model is 1.01, and the standard deviation is 0.09. Good agreement was achieved between test results and prediction results from the SSTM.

• The means for the strength ratios of the test value to the theoretical value calculated by the American Code (ACI 318 and AISC 1999) and British Code (BS 8110) are 1.16 and 1.23, respectively, and the standard deviation is 0.32. The calculated results are safe and in good agreement with the experimental values although they are more discrete than the V_{test}/V_{cal} calculated by the softened strut-and-tie model.

• The standard deviation and coefficient of variation calculated from the softened strut-and-tie model are the lowest. The method includes a definite mechanical model, and it can reasonably reflect the failure

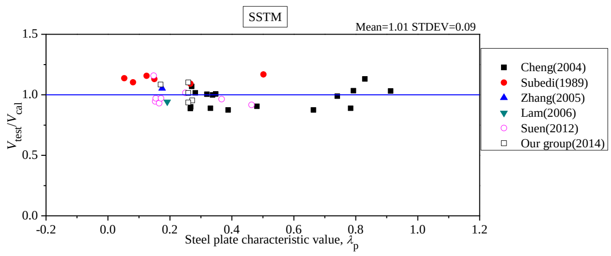

(a) SSTM (Method 1)

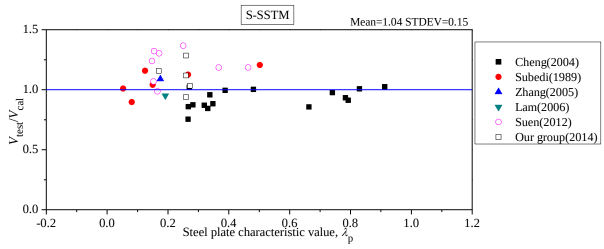

(b) S-SSTM (Method 2)

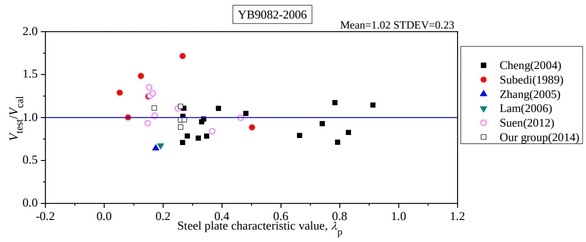

(c) YB9082-2006 (Method 3)

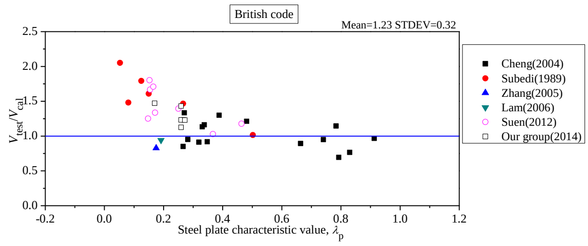

(d) British Code (BS 5950 and BS 8110) (Method 4)

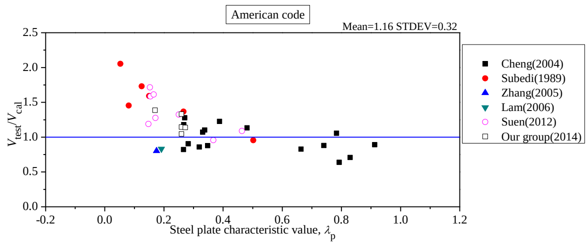

(e) American Code (ACI 318 and AISC 1999) (Method 5)

Fig. 14 Shear strength ratio versus steel plate characteristic values

mechanisms of PRC coupling beams with a span-to-depth ratio not exceeding 2.5.

Acknowledgements

The work reported in this paper was supported by the National Natural Science Foundation of China (Grant No. 51608441, Grant No. 51478382), China Postdoctoral Science Foundation (Grant No. 2017M613174), Natural Science Basic Research Plan in Shaanxi Province of China (Grant No. 2017JQ5032) and Young Talent fund of University Association for Science and Technology in Shaanxi, China (Grant No. 20170513). The authors express their sincere gratitude to the sponsors.

References

ACI 318 (2014), Building Code Requirements for Structural Concrete and Commentary, American Concrete Institute; Michigan, USA.

AISC (1999), Load and Resistance Factor Design Specification for Structural Steel Buildings, American Institute of Steel Construction, Michigan, USA.

BS 8110 (1997), Code of Practice for Design and Construction. Part 1, Structural Use of Concrete, British Standard Institution; London, UK.

Cheng, P.C. (2004), "Shear capacity of steel-plate reinforced concrete coupling beams", The Hong Kong University of Science and Technology, Hong Kong.

Collins, M.P. (1986), "A rational approach to shear design-the 1984 Canadian code provisions", *J. Neurosci.*, **83**(6), 925-33.

Foster, S.J. and Malik, A.R. (2002), "Evaluation of efficiency factor models used in strut-and-tie modeling of nonflexural members", *J. Struct Eng.*, **128**(5), 569-577. https://doi.org/10.1061/(ASCE)0733-9445(2002)128:5(569).

Habib, A.B. and Roja, M.A. (2016), "Performance based evaluation of RC coupled shear wall system with steel coupling beam", *Steel Compos. Struct.*, **20**(2), 337-355. http://dx.doi.org/10.12989/scs.2016.20.2.337.

Hoang, L.C. and Nielsen, M.P. (1998), "Plasticity approach to shear design", *Cement Concrete Compos.*, **20**(6), 437-453. https://doi.org/10.1016/S0958-9465(98)00026-2.

Hou, W. (2018), "Seismic performance of steel plate reinforced high toughness concrete coupling beams with different steel plate ratios", *Compos. Part B.*, **159**, 199-210. https://doi.org/10.1016/j.compositesb.2018.09.100.

Hsu, T.T.C. and Mo, Y.L. (2010), *Unified Theory of Concrete Structures*, A John Wiley and Sons Ltd., Singapore.

Hwang, S.J., Fang, W.H., Lee, H.J. and Yu, H.W. (2001), "Analytical model for predicting shear strength of squat walls", *J. Struct Eng.*, **127**(1), 43-50. https://doi.org/10.1061/(ASCE)0733-9445(2001)127:1(43).

Lam, W.Y. (2006), "Plate-reinforced composite coupling beams: experimental and numerical studies", The University of Hong Kong, Hong Kong.

Lian, M., Su, M.L. and Guo, Y. (2017), "Experimental performance of Y-shaped eccentrically braced frames fabricated with high strength steel", *Steel Compos. Struct.*, **24**(4), 441-453. https://doi.org/10.12989/scs.2017.24.4.441.

Liang, X.W. and Xing, P.T. (2018), "Seismic behavior of fiber reinforced cementitious composites coupling beams with conventional reinforcement", *Earthq. Struct.*, **14**(3), 261-271.

https://doi.org/10.12989/eas.2018.14.3.261.
Park, S. and Mosalam, K.M. (2012), “Analytical model for predicting shear strength of unreinforced exterior beam-column joints”, *ACI Struct. J.*, **109**(2), 149-160.
Ramirez, J. and Breen, J. (1991), “Evaluation of a modified truss model approach for beam in shear”, *ACI Struct. J.*, **88**(5), 562-571.
Seongwoo, G., Myoungsu, S., Benjamin, P. and Deokjung, L. (2014), “Nonlinear modeling parameters of RC coupling beams in a coupled wall system”, *Earthq. Struct*., **7**(5), 817-842. http://dx.doi.org/10.12989/eas.2014.7.5.817.
Subedi, N.K. (1989), “Reinforced concrete beams with plate reinforcement for shear”, *Proc. Inst. Civil Eng., Part Res. Theor.*, **87**(3), 377-399. https://doi.org/10.1680/iicep.1989.2972.
Subedi, N.K. and Baglin, P.S. (1997), “Plate reinforced concrete beams: experimental work”, *Eng. Struct*., **21**(3), 232-254. https://doi.org/10.1016/S0141-0296(97)00171-5.
Suen, P.C. (2012), “Steel-plate encased concrete coupling beams”, The Hong Kong University of Science and Technology, Hong Kong.
Thorburn, L.J., Kulak, G.L. and Montgomery, C.J. (1983), “Analysis of steel plate shear walls”, Structural Engineering Report No. 107, University of Alberta, Edmonton.
Tian, J.B., Wang, Y.C. and Li, S. (2019), “Seismic performance and design method of PRC coupling beam-hybrid coupled shear wall system”, *Earthq. Struct*., **16**(1), .83-96.. https://doi.org/10.12989/eas.2019.16.1.083.
Tsonos, A.G. (2007), “Cyclic load behaviour of reinforced concrete beam-column subassemblages of modern structures”, *ACI Struct. J.*, **194**(4), 468-478. https://doi.org/10.2495/ERES050421.
Wang, P. and Shi, Q.X. (2015), “Experimental behavior and shear bearing capacity calculation of RC columns with a vertical splitting failu”, *Earthq. Struct*., **9**(6), 1233-1250. http://dx.doi.org/10.12989/eas.2015.9.6.1233.
Wang, P., Shi, Q.X. and Wang, F. (2017), “Experimental investigation of SRHSC columns under biaxial loading”, *Earthq. Struct*., **13**(5), 485-496. https://doi.org/10.12989/eas.2017.13.5.485.
Wong, H.F. and Kuang, J.S. (2014), “Predicting shear strength of RC interior beam-column joints by modified rotating-angle softened-truss model”, *Comput. Struct.*, **133**(3), 12-17. https://doi.org/10.1016/j.compstruc.2013.11.008.
Xing, G.H., Liu, B.Q. and Wu, T. (2011), “Shear strength of reinforced concrete frame joints using softened strut and tie model”, *J. Build Struct.*, **32**(5), 125-134.
Zhang, G. (2005), “Experimental study on seismic behavior of steel plate reinforced concrete coupling beams”, Tsinghua University, Beijing, China.
Zhang, L.X. and Hsu, T.T.C. (1998), “Behavior and analysis of 100 MPa concrete membrane elements”, *J. Struct Eng.*, **124**(1), 24-34. https://doi.org/10.1061/(ASCE)0733-9445(1998)124:1(24).

AT